Improving the accuracy of a Shack-Hartmann wavefront sensor on extended scenes

M Rais[1,2], J-M Morel[2], C Thiebaut[3], J-M Delvit[3] and G Facciolo[2,4]

[1] TAMI, Universitat des les Illes Balears, Spain
[2] CMLA, ENS-Cachan, Université Paris Saclay, France
[3] Centre National des Études Spatiales, France
[4] LIGM, UMR 8049, École des Ponts, UPE, France

E-mail: martin.rais@cmla.ens-cachan.fr

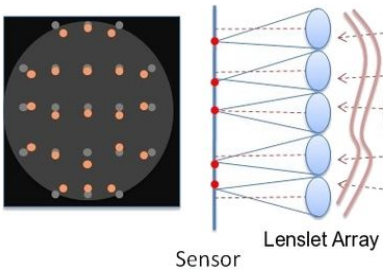
Abstract. In order to achieve higher resolutions, current earth-observation satellites use larger lightweight main mirrors which are usually deformed over time, impacting on image quality. In the context of active optics, we studied the problem of correcting this main mirror by performing wavefront estimation in a closed loop environment. To this end, a Shack-Hartman wavefront sensor (SHWFS) used on extended scenes could measure the incoming wavefront. The performance of the SHWFS on extended scenes depends entirely on the accuracy of the shift estimation algorithm employed, which should be fast enough to be executed on-board. In this paper we specifically deal with the problem of fast accurate shift estimation in this context. We propose a new algorithm, based on the global optical flow method, that estimates the shifts in linear time. In our experiments, our method proved to be more accurate and stable, as well as less sensitive to noise than all current state-of-the-art methods.

1. Introduction

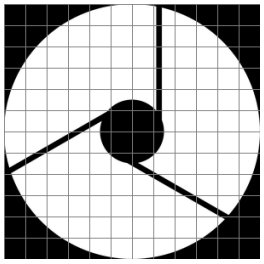
Adaptive optics was originally developed for the field of astronomy to remove image aberrations induced by wavefronts propagating through Earth's atmosphere. Its task is to correct the aberrations of an incoming wavefront by using a deformable mirror in order to compensate for the distortion. It has been shown that adaptive optics allows to reduce these aberrations thus improving the image quality [1].

A key component of an adaptive optics system is the wavefront sensing mechanism. In astronomical imaging a wavefront sensing device is frequently used in conjunction with a deformable mirror in order to correct the undesired effects of atmospheric turbulence, thus improving the quality of sensed images. A Shack-Hartmann wavefront sensor (SHWFS) is one of such devices. It uses an array of lenslets to measure the deformation of the incoming wavefront. The shift of each lenslet focal plane image is proportional to the mean slope of the wavefront in the subaperture onto this lenslet, thus allowing to obtain a discrete local approximation of the slope of the wavefront, as shown in Fig. 1a. The measured slopes are then used to approximate the actual wavefront. This deformation is usually measured using point sources such as a star.

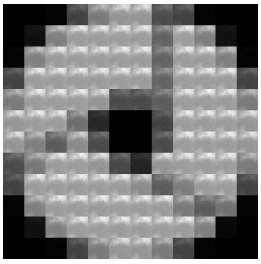
Adaptive optics can also be applied in the context of earth-observation satellites [2, 3]. In this setting, the problem of atmospheric turbulence is negligible. However, lightweight mirrors are required to increase the resolution, since mission costs are driven by the payload weight. The drawback of such mirrors is that time-varying deformations due to thermal effects and vibration



(a) Local shifts in the SHWFS



(b) Occlusions in a SHWFS



(c) Example images

Figure 1: Left: A SHWFS measures the wavefront by computing the local shifts between the detected spots (in red) and the reference spots (in grey), which would occur if no deformation is present. Right: A SHWFS occlusion schema using a Korsch telescope. The secondary mirror and the arms used to hold it are clearly visible. The decrease of the incoming signal for each lenslet is proportional to its occlusion.

deteriorate the image quality [4]. In adaptive optics a SHWFS device is used together with a deformable mirror to compensate for these aberrations.

There are some key differences between using wavefront sensing for earth-observation satellites and for astronomical observation. First, the SHWFS needs to be used on extended scenes, rather than source points. This yields a grid of images, one for each sub-aperture, which are shifted versions of the same scene. Second, the pupil of the Korsch telescope in the satellite is generally occluded in the center by a secondary mirror and the arms used to hold it. In these regions, the sub-apertures suffer a loss in the incoming signal, proportional to their percentage of occlusion (Fig. 1b), which results in the output depicted in Fig. 1c. Third, satellites have limited computational capacity which constrains the shift estimation task, making several shift estimation methods not suitable to be implemented on-board due to their high complexity.

Our contribution is threefold. First, an analysis of the *state-of-the-art* on wavefront correction through the use of SHWFS on extended scenes is performed (section 2). Second, we propose the use of an iterative global optical flow method for shift estimation (section 3) which presents several advantages over the conventional correlation methods. Finally, in section 4, a thorough evaluation of the discussed methods and our proposed algorithm is performed, evaluating their robustness to noise and image characteristics. Our conclusions are reported in section 5.

2. State-of-the-art review

Since the SHWFS was introduced in the late 1960s [5], several algorithms were proposed to estimate the shifts using point sources (like stars). However, only few authors have studied the problem when the source is extended, as when observing the earth from space. They can be organized in: Correlation methods which compute cross-correlation either in the space [6, 7, 8] or frequency domain [2, 9, 10, 11, 8] by assuming periodicity. Phase correlation methods estimate the shift directly in the frequency domain [11, 12] by fitting a plane to the phase correlation matrix between both images. The iterated methods [9, 10] progressively improve the estimation. Lastly, maximum likelihood (ML) approaches [13] incorporate specific noise models, and often lead to an optimization problem. Although it improves over correlation, ML is usually not considered for SHWFS [7, 2] because of its high computational cost.

Correlation-based Methods. These methods compute a correlation score on a grid $C(i, j)$ and interpolate it to determine the subpixel location of the peak. The methods mainly differ in the choices of correlation score and interpolation strategy. Michau et al. [6] was among the first to propose an experimental implementation for using a Shack-Hartmann sensor on extended sources. They compute the discrete cross-correlation of the two images, and estimate the subpixel shift by taking the centroid of the shifts with higher correlation value.

Löfdahl [8] tested several shift estimation algorithms considering several sources of errors such as noise, blur and bias mismatch. For the scores $C(i,j)$ he considered the sum of squared differences between the subimages (SDF), covariance in Fourier (CFI), a trend-corrected covariance (CFF) , the sum of the absolute differences (ADF), and its square (ADF^2). Subpixel shifts are computed by fitting a conic section around the minimum correlation value on the grid $C(i_{min}, j_{min})$, or by fitting parabolas independently in each dimension. For Gaussian noise, the authors choose SDF followed by fitting a 2D conic into the 3×3 values (SDF-2QI).

Poyneer [2] also evaluated several methods, including ML and a variant of phase correlation, but in the end opted for a similar Least Squares approach (using periodic-convolution computed in the Fourier domain) followed by 1D parabolic fitting.

Phase Correlation. Phase-correlation [12, 11] methods can estimate the shift directly in the frequency domain. In a noiseless situation, for an $M \times N$ image $f(x,y)$ the Fourier shift theorem yields $g(x,y) = f(x-\Delta_x, y-\Delta_y) = \mathcal{F}^{-1}(F(u,v)\exp(-j2\pi(\frac{u\Delta_x}{M} + \frac{v\Delta_y}{N})))$. Hence, the normalized cross-power spectrum between f and its shifted version g, given by $\frac{F(u,v)G^*(u,v)}{|F(u,v)G^*(u,v)|} = \exp(j2\pi(\frac{u\Delta_x}{M} + \frac{v\Delta_y}{N}))$, allows to compute the phase correlation matrix $\phi(u,v) = 2\pi(\frac{u\Delta_x}{M} + \frac{v\Delta_y}{N})$ for each frequency. The shifts can then be directly estimated in the frequency domain by fitting a plane passing through the origin of the computed correlation matrix [12]. To avoid aliased frequencies, Knutsson *et al.* [11] (also [9]) propose to discard most of the frequencies keeping only the two, or the four lowest frequencies, resulting in a fast method that does not require computing the whole FFT. The choice of two frequencies also has the advantage of being the least sensitive to aliasing [12], hence is the most reliable, but more sensitive to noise. Using more frequency components instead yields more robustness to noise.

Iterated Estimation. Sidick et al. [9] proposed ACC (Adaptive Cross-Correlation), an iterative method that estimates the shift in the Fourier domain by phase correlation [12]. Similarly to Knutsson et al. [11] only low frequencies are used to estimate the shift (just 8 coefficients). At each iteration, the second image is resampled (in the frequency domain) by the current shift estimate. This method attains very low errors of the order of 0.05 pixels by using fewer than 6 iterations. The same authors later [10] replaced the shift estimation with the periodic-correlation technique of [2] with parabolic fitting around the peak. The resulting method (APC) is more robust to noise than ACC.

3. Accurate shift estimation using optical flow

In order to estimate the shift between two sub-apertures, we propose to use a gradient-based shift estimator (GBSE) based on the optical flow equation. This technique, originally proposed by Lucas and Kanade [14], relates the difference between two successive frames to the spatial intensity gradient of the first image. Given the two images $I_2(x,y) = I_1(x-v_x, y-v_y)$ related by the translation (v_x, v_y), a first order Taylor approximation of I_1 yields the linear relation

$$I_1(x,y) - I_2(x,y) \approx v_x \frac{\partial I_1(x,y)}{\partial x} + v_y \frac{\partial I_1(x,y)}{\partial y}. \tag{1}$$

The displacement between I_1 and I_2 is estimated by computing the least squares solution

$$\begin{bmatrix} v_x \\ v_y \end{bmatrix} = \begin{bmatrix} \sum I_x^2 & \sum I_x I_y \\ \sum I_x I_y & \sum I_y^2 \end{bmatrix}^{-1} \begin{bmatrix} \sum I_x I_t \\ \sum I_y I_t \end{bmatrix}, \tag{2}$$

where I_x, I_y stands for $\frac{\partial I_1}{\partial x}$ and $\frac{\partial I_1}{\partial y}$ respectively, and $I_t = I_1 - I_2$ is the derivative over time.

It is important to remark that by centering the Taylor development at 0 and taking up to the first order term, the method gets systematically biased, directly affecting its accuracy. Furthermore, the noise in the input images is ignored by the algorithm, which also impacts on its performance. Both these bias sources are studied in detail in [15].

Iterative gradient-based shift estimator. Instead of dealing with the bias explicitly, Pham et al. [15] show that both bias sources depend linearly on the shift magnitude. This justifies the use of an iterative method, which is able to significantly reduce the bias, provided an appropriate resampling method is used. This algorithm is described in the following lines:

$i \leftarrow 0;\ I_2(0) \leftarrow I_2;\ w \leftarrow 0$
while $i < k$ **and** $|v(i-1) - v(i-2)| \geq \tau$ **do**
  $v(i) \leftarrow findshift(I_1, I_2(i))$ // Eq. (2)
  $w \leftarrow w + v(i)$ // Accumulate total shift
  if $i + 1 < k$ **then**
    $I_2(i+1) \leftarrow Shift(I_2, -w)$ // Resample the original I_2 by shifting it $-w$ pixels
  $i \leftarrow i + 1$

where k is the maximum amount of iterations, τ is a parameter that indicates the minimum incremental shift to stop iterating, $findshift$ uses Eq. (2) to solve for $v(i)$ and $Shift$ resamples an image by interpolation (see section 4).

Gradient computation. Several gradient estimation methods were tested and, due to the inherent noise in the input images, the Gaussian derivatives offered the best performance. Note that since our shift estimation is focused on accuracy and we are dealing with small images, using a larger kernel for computing the image derivatives imply discarding more boundary pixels, thus leaving fewer pixels to estimate the shift in Eq. (2).

Image intensities equalization. One requirement of the GBSE algorithm is to work on images with similar intensities. Since occluded sub-apertures receive less light, their intensities differ from the reference image. To this end, a simple intensity equalization applied. All subimages are equalized by scaling their mean to the highest mean among all subapertures, $I_k(x, y) = [\max_j(\mu_j)/\mu_k]I_k(x, y)$ where μ_k is the average value of image k.

4. Results

Experimental Setup. A simulator was used to evaluate the performance of the proposed method. Given a 12-bit input image, a set of images was generated matching a SHWFS configuration provided by CNES. A 12×12 lenslet grid occluded as shown in Fig. 1b was assumed. For each lenslet a ground truth shift was randomly generated. Since we were simulating in a closed loop environment, the maximum displacement was kept to half a pixel. Each sub-aperture image was then obtained by resampling the input image in Fourier, extracting a 37×37 pixels subimage, multiplying by the occlusion factor, and lastly adding the noise.

This setup permits compare SHWFS algorithms only considering the shifts induced by the wavefront slope. However, it has to be noted that due to phenomena such as scintillation and phase anisoplanatism, the relationship between the real wavefront aberration and the observed images may be more complex than shifts between the lenslet images.

The error for each method was computed as the mean error for all valid sub-apertures (less than 60% of its surface is occluded). The error for each sub-aperture is the Euclidean distance between the measured and the ground truth shift. To evaluate the robustness to image content, we used three subimages: a highly contrasted one that should not present any difficulty for shift estimation, a slightly more challenging one with its gradient mainly distributed on a single direction, and one from the sea with almost no signal. Different amounts of additive white Gaussian noise were simulated (with standard deviation $\sigma \in [1, ..., 150]$), and all methods were evaluated on 100 noise realizations. Fig. 2 shows the subimages affected by three noise levels. Signal dependent noise was handled by application of a variance stabilization transform.

We tested several variants of the proposed GBSE method. Five interpolation methods for resampling, namely bilinear, bicubic, cubic spline and Fourier (using the Fourier shift theorem), with and without image symmetrization, three values for the Gaussian derivative

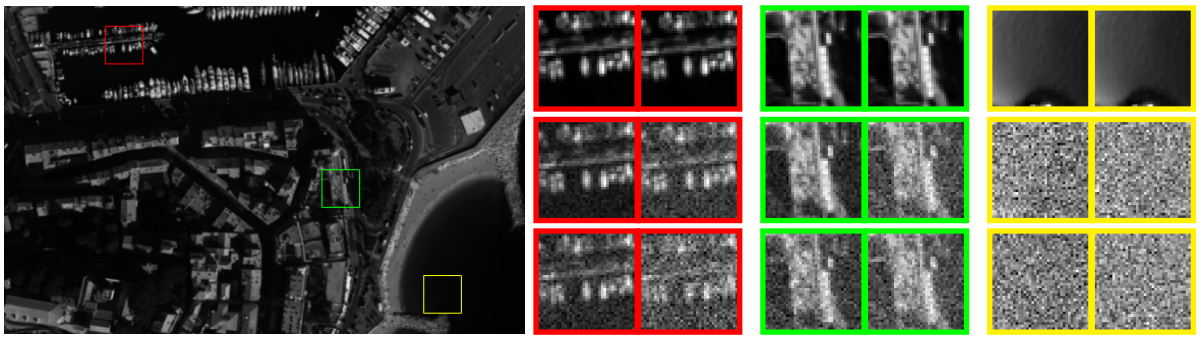


Figure 2: Left: Input image used for the simulation. Right: For each level of noise $\sigma = \{1, 100, 200\}$ (vertically separated), two different sub-apertures are shown: no occlusion and 57% occluded (horizontally separated). The dynamic ranges were stretched for viewing purposes.

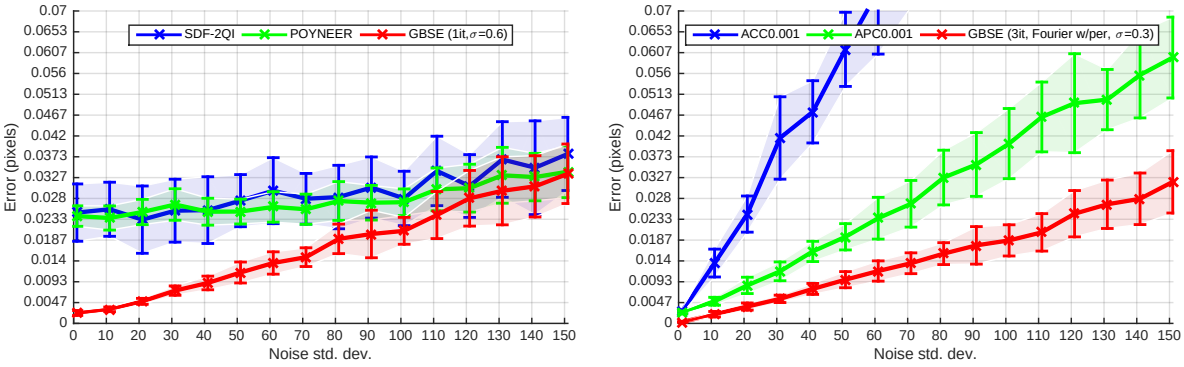


Figure 3: Performance for non-iterative and iterative methods on first test image.

width $\sigma = \{0.3, 0.6, 1\}$, and using up to three iterations per shift estimation. From these methods we retained the best performing non-iterative method ($k = 1$ and no resampling) which uses $\sigma = 0.6$ for the gradient computation, and the best with 3 iterations which uses Fourier resampling with image periodization and $\sigma = 0.3$. We compared them with the best performing state-of-the-art algorithms, namely, ACC [9], APC [10], the method from Poyneer [2] and the SDF-2QI algorithm from Löfdahl [8].

It should be noted that if a single iteration is used, the gradient estimation with $\sigma = 0.6$ gives better results than using $\sigma = 0.3$. This is because a higher σ removes more noise from the derivatives, and blurring the images impacts less on the accuracy than not taking care of the noise. This noise influence can be reduced by iterating the method [15], which justifies estimating the gradient from a sharper image on those cases.

Results and discussion. We compared iterative and non-iterative algorithms separately. The average errors for non-iterating methods on the first image type are shown in Fig. 3 (left). The non-iterative GBSE outperforms both Poyneer and SDF-2QI (which perform similarly in this image), GBSE is also more stable (less variability). In Fig. 3 (right) both iterative methods ACC and APC were compared with our GBSE using 3 iterations. Again the proposed method is the most accurate and more stable. Even more, this method is the best also compared to non-iterated methods. We also note that ACC is not much robust to noise. This is a well-known problem for phase-correlation methods which use a limited number of frequencies [16].

The results for the second image type (Fig. 4) are similar to the first one, although the average errors are higher. While the SDF-2QI performs slightly worse, the Poyneer method is considerably worse. This is due to discrepancies at the image boundaries resulting from the periodicity assumption of the periodic convolution used by Poyneer. This is also explains why the ACC method behaves so poorly on this image. Yet again, the proposed methods are more precise, stable and with less variability than the state-of-the-art. Finally, for the third image

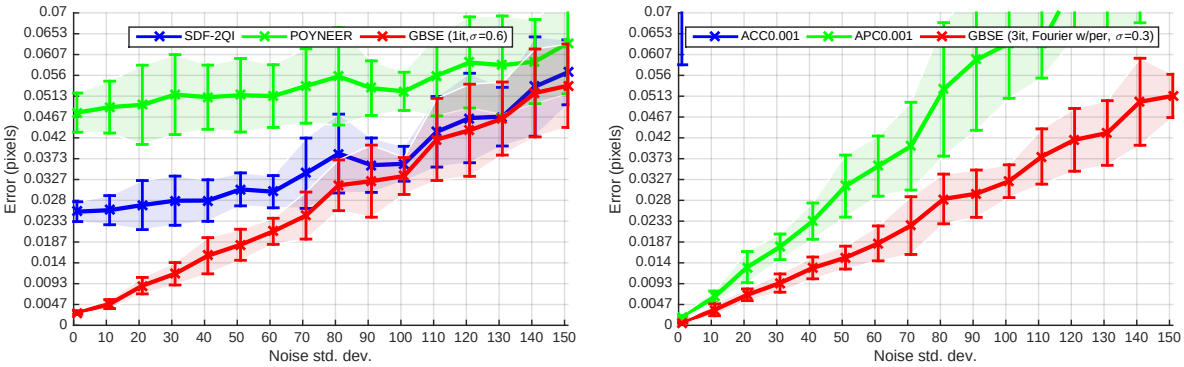


Figure 4: Performance for non-iterative and iterative methods on second test image.

type all the methods fail so the graph is omitted.

5. Conclusion

A new method for accurate sub-pixel shift-estimation, based on an iterative global optical flow algorithm, is proposed in the context of a SHWFS on extended scenes for aberration correction on-board earth-observation satellites. Simulations using plausible information provided by CNES show that the proposed algorithm is more accurate, stable, robust to noise, and with lower variability than the current state-of-the-art, permitting a more precise wavefront estimation.

Acknowledgments

Work partly founded by the Centre National d'Etudes Spatiales (CNES, MISS Project) and the Office of Naval research (ONR grant N00014-14-1-0023). During this work, Martin Rais had a fellowship of the Ministerio de Economia y Competividad (Spain), reference BES-2012-057113, for the realization of his Ph.D. thesis.

References

[1] Wizinowich P *et al.* 2000 *Publications of the Astronomical Society of the Pacific* **112** 315–319
[2] Poyneer L A 2003 *Applied Optics* **42** 5807–5815
[3] Bonnefois A *et al.* 2014 Comparative theoretical and experimental study of a Shack-Hartmann and a Phase Diversity Sensor, for high-precision wavefront sensing dedicated to Space Active Optics *ICSO 2014*
[4] Chen P C, Bowers C W, Marzouk M and Romeo R C 2000 *Optical Engineering* **39** 2320–2329
[5] Platt B C *et al.* 2001 *Journal of Refractive Surgery* **17** S573–S577
[6] Michau V, Rousset G and Fontanella J 1993 Wavefront sensing from extended sources *Real Time and Post Facto Solar Image Correction* vol 1 p 124
[7] Michau V, Conan J M, Fusco T, Nicolle M, Robert C, Velluet M T and Piganeau E 2006 Shack-hartmann wavefront sensing with extended sources *SPIE Optics+Photonics* (SPIE) pp 63030B–63030B
[8] Löfdahl M G 2010 *Astronomy & Astrophysics* **524** A90
[9] Sidick E *et al.* 2007 An Adaptive cross-correlation algorithm for extended scene Shack-Hartmann wavefront sensing *Adaptive Optics: Methods, Analysis and Applications* (OSA)
[10] Sidick E 2011 Adaptive periodic-correlation algorithm for extended scene shack-hartmann wavefront sensing *Imaging and Applied Optics* (Optical Society of America) p CPDP1
[11] Knutsson P, Owner-Petersen M and Dainty C 2005 *Optics express* **13** 9527–9536 ISSN 1094-4087
[12] Stone H, Orchard M, Chang E C and Martucci S 2001 *Geoscience and Remote Sensing, IEEE Transactions on* **39** 2235–2243 ISSN 0196-2892
[13] Gratadour D, Mugnier L and Rouan D 2005 *Astronomy & Astrophysics* **443** 357–365
[14] Lucas B D and Kanade T 1981 An iterative image registration technique with an application to stereo vision IJCAI'81 (Morgan Kaufmann Publishers Inc.) pp 674–679
[15] Pham T Q, Bezuijen M, Van Vliet L J, Schutte K and Hendriks C L L 2005 Performance of optimal registration estimators *Proc. SPIE* vol 5817 pp 133–144
[16] Gilman A and Leist A 2013 Global Illumination-Invariant Fast Sub-Pixel Image Registration pp 95–100 ISBN 978-1-61208-283-7